

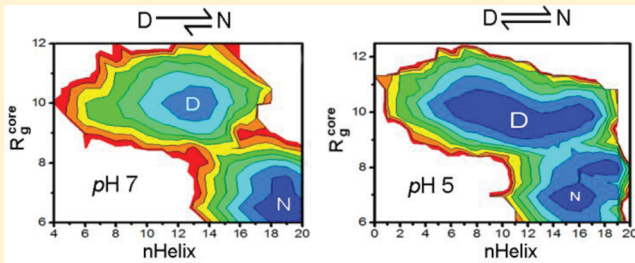
Effects of Two Solvent Conditions on the Free Energy Landscape of the BBL Peripheral Subunit Binding Domain

Hanzhong Liu and Shuanghong Huo*

Gustaf H. Carlson School of Chemistry and Biochemistry, Clark University, Worcester, Massachusetts 01610, United States

Supporting Information

ABSTRACT: BBL is a small independently folding domain with two main parallel helices. The experiment of C^α secondary shifts has shown that changing the pH from ~ 7 to ~ 5 results in the reduced helicity at the C-terminus of helix 2. Combining constant pH molecular dynamics with replica exchange, we sampled the protein conformation space and protonation states extensively under a neutral pH condition and an acidic condition. Our results reveal that the solvent conditions influence the free energy landscape. Under the neutral pH condition, the denatured state and the native state are well separated. The condition of the acidic pH reshapes the free energy surface, leading to a broadly populated denatured-state basin and a low free energy barrier between the denatured state and the native state. The acidic pH shifts the equilibrium between the denatured state and the native state in favor of the denatured state. Caution must be used to interpret experimental data under the acidic condition because the contribution of the denatured state is significant. Our simulation results are supported by the fact that the calculated chemical shifts are in good agreement with the experiment data.



INTRODUCTION

BBL belongs to the family of 2-oxo-acid dehydrogenase peripheral subunit binding domains.¹ The solution structure of this independently folding domain at neutral pH and 200 mM of ionic strength shows a three-helix bundle: two main parallel helices (Helix 1 and Helix 2) and a short 3_{10} helix (Figure 1).² The recent experiment on pH titration of individual residues has shown that the two histidine residues, His142 on Helix 1 and His166 on Helix 2, exhibit different pK_a values,³ 6.47 and 5.39, respectively. In addition, the data of C^α secondary shifts³ and molecular dynamics (MD) simulations⁴ have revealed that changing the pH from ~ 7 to ~ 5 shifts the native state of the protein from an ordered conformation with high helicity to a less ordered state with lower helicity. On the basis of these results, it was proposed that the native state of BBL is heterogeneous, and the heterogeneity is the origin of the asynchronous unfolding behavior of this protein;⁴ specifically, different parts of the protein exhibit different transition midpoint temperatures. This behavior was previously interpreted as noncooperative downhill folding.⁵

Although different groups have different views on the folding mechanism of this protein, downhill folding versus two-state folding,^{2,7} a consensus in literature is that solvent conditions play a crucial role in determining the folding cooperativity⁸ and native structure.⁴ This implies that the (free) energy landscape varies with solvent conditions. A recent study on the folding pathways of BBL suggests that there are parallel routes to the native state, and the relative predominance of the folding pathways may vary with solvent conditions.⁹ A G_0 model simulation that includes the many-body interactions demonstrates that the fine-tune in

the protein construct and solvent conditions result in the differences in the levels of folding cooperativity.¹⁰ The all-atom MD simulations of the native state of BBL under four solvent conditions, pH 7 with and without salt and pH 5 with and without salt, show that the pH influences the native structure significantly, while the salt effect is relatively small under these two pH conditions.⁴

In traditional MD simulations, the protonation state of every titratable residue is fixed. For example, both His142 and His166 are unprotonated at pH 7 and protonated at pH 5 in the work of Settanni et al.⁴ Ideally, simulations should sample both molecular conformations and protonation states because they are highly coupled.¹¹ Constant pH simulation is an active research area in which efforts have been made to treat the protonation states as variables and to treat the pH as a fixed parameter.¹² This kind simulation method is desirable to obtain the right population of different protonation states for certain residues when their pK_a values are close to the solution pH and/or when the residues are surrounded by several other titratable groups.

To study the acidic pH induced conformational change of BBL, we employed the constant pH molecular dynamics (CPHMD)¹³ implemented in CHARMM(c35b2).¹⁴ This approach is an extension of λ -dynamics.¹⁵ It combines an all-atom description of protein¹⁶ and a generalized Born (GB) implicit solvent model.¹⁷ Using the terminology of λ -dynamics, the value of a continuous titration coordinate (λ) ranges from 0 to 1. Zero represents a

Received: October 11, 2011

Revised: November 20, 2011

Published: November 29, 2011

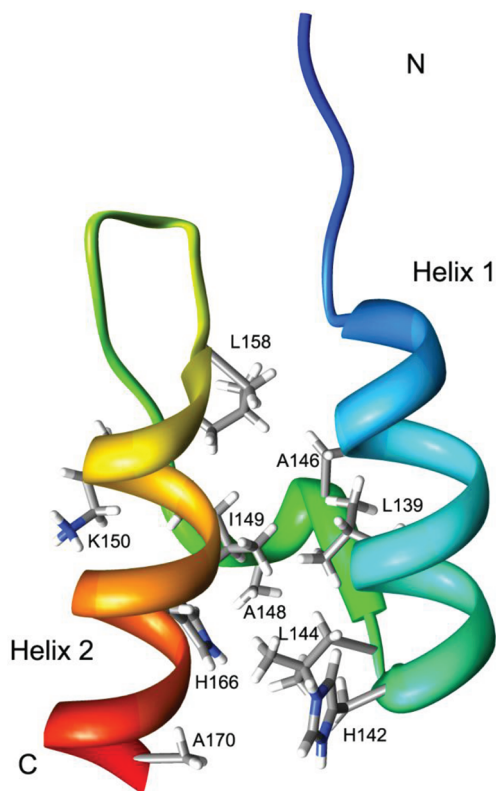


Figure 1. NMR structure of BBL (PDB ID: 1W4H, model 1) at neutral pH. There are 45 amino acids, residue 126 to residue 170. Helix 1 is from Pro133 to His142, and Helix 2 ranges from Arg160 to Lys169. The structure is plotted using Chimera.⁶ The residues within 6 Å of His 166 (excluding the nearest three neighbors in sequence) are shown explicitly. The coloring scheme for atoms is N (blue), C (gray), H (white), and O (red).

protonated state, and 1 is an unprotonated state, and anything in between is in a mixing state. λ is treated as a fictitious particle with its mass equivalent to a heavy atom. The titration coordinate propagates simultaneously with the atomic motions of BBL. Biassing potentials are introduced to suppress the population in the mixing state. To extensively sample the conformation space and the protonation states, we use CPHMD combined with replica exchange.¹⁸ The traditional MD simulations revealed some overall structural changes in the native state ensemble of the protein upon lowering the pH, such as the distributions of root-mean-square deviation (rmsd) and native contacts.⁴ How do solvent conditions affect the free energy landscape? Our goal is to investigate the feature of free energy landscape under different solvent conditions and to interpret the experimental C^α secondary shifts from the free energy landscape point of view.

METHODS

The initial structure of our simulations is the NMR structure (Model 1 of 1W4H²) resolved at a pH of 7.0 and an ionic strength of 200 mM. The acetyl and *N*-methyl groups were patched at the N-terminus and C-terminus, respectively. Two simulations of replica exchange constant pH molecular dynamics (REX-CPHMD) were performed: one is under pH 5 without salt, and the other is under pH 7 with 0.2 M of salt. We chose these two solvent conditions because they are the two conditions under which discrepant behaviors of folding were observed.²⁷ Our

goal is to uncover the free energy landscape under these two commonly used solvent conditions in experiments, rather than to distinguish between the salt effect and the pH effect. For the latter goal, CPHMD simulations with explicit water and salt are required because the salt effect on protein secondary structure is complex.¹⁹ Currently, CPHMD is limited to the implicit solvent model in CHARMM (c35b2).¹⁴

To reduce the population of mixed titration and tautomeric states, a titration barrier of 1.75 kcal/mol and a tautomeric interconversion barrier of 2.5 kcal/mol were set. The cutoff distance for nonbonded interactions is 24 Å. The replica exchange simulation was carried out using the MMTSB Tool set.²⁰ The temperature range was set from 273 to 625 K based on the previous replica exchange MD simulations of BBL with fixed protonation states²¹ and our “training” simulations in different temperature ranges. To maintain an ~40% exchange rate between the replicas adjacent in the temperature space, 24 replicas were used to realize the random walk in the temperature space and rmsd space (see Supporting Information). The exchanges were attempted every 2 ps. The optimal temperature range and exchange rate allow several events of unfolding and refolding to occur during our simulations (see Supporting Information). Each simulation began with 200 steps of minimization, which includes 50 steps of steepest descent followed by 150 steps of adopted-basis Newton–Raphson with harmonic restraints on all of the heavy atoms. The restraints were subsequently removed, and the minimization was continued for an additional 850 steps: 50 steps of steepest descent, and then 800 steps of adopted-basis Newton–Raphson. This minimization was followed by the dynamics that were propagated using the Langevin algorithm with the friction coefficient equal to 5 ps⁻¹. The lengths of covalent bonds involving hydrogen atoms were constrained with the SHAKE algorithm²² to allow a time step of 2 fs. Prior to the production run, 300 ps of initialization and 300 ps of equilibration were carried out. The snapshots for analysis were saved every 2 ps over the 50 ns of production run for each replica, for a total of 1.2 μs of simulation under each solvent condition.

The fractional population of the unprotonated state of a titratable group, also called unprotonated fraction, is defined as^{13b}

$$S = \frac{N^{\text{unprot}}}{N^{\text{unprot}} + N^{\text{prot}}} \text{ and } \begin{cases} \lambda < 0.1, & \text{protonated} \\ \lambda > 0.9, & \text{unprotonated} \end{cases}$$

where N^{unprot} and N^{prot} are the occurrence of the unprotonated state and protonated state in the ensemble, respectively, and λ is the titration coordinate. The cutoff value of λ is the result of trade-off between a strict definition of protonation and good statistics. Most strictly, a residue is protonated only when $\lambda = 0$, but this definition will result in not enough data for good statistics within a 1 ns window. With our cutoff, there are no more than 20% conformations in the mixed state of protonation ($0.1 < \lambda < 0.9$) for each 1 ns window. By calculating S as a function of time, we can monitor how the titration states of the two histidine residues change dynamically.

We employed PTWHAM²³ implemented in the MMTSB Tool set to obtain the profile of the potential of mean force (PMF) and the weighted average value of simulation observables (including helicity, interhelical angle, and side-chain contacts) and chemical shifts. SHIFTX (version 1.1)²⁴ was used to estimate the C^α chemical shifts of each simulation structure along the last 20 ns trajectory of each replica. The predicted C^α secondary chemical shifts were obtained by subtracting the chemical shift values of random

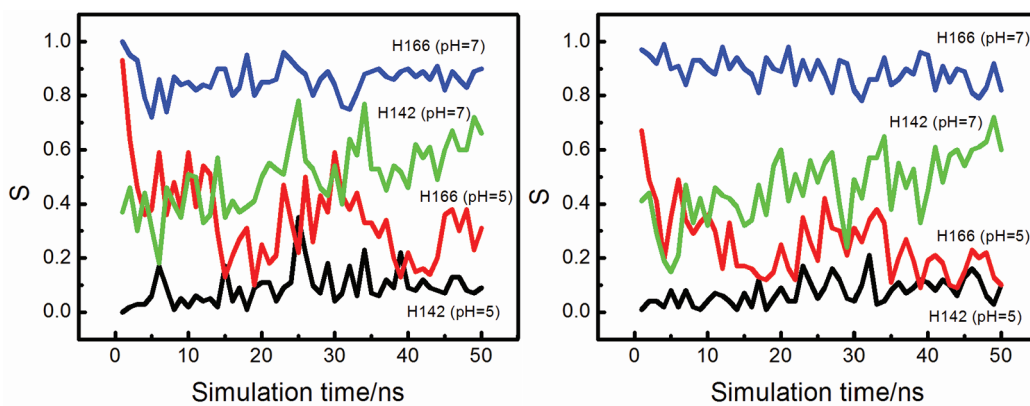


Figure 2. Unprotonated fraction (S) as a function of time for the pseudotrajectories under 293 K (left) and 304 K (right).

coils from the corresponding calculated C^α chemical shifts. Nateness (Q) is defined as the fractional number of native residues. If the (ϕ, ψ) angles of a given residue is within $\pm 30^\circ$ of their native-state values, then this residue is considered as a native residue. Because the N-terminus of BBL is very flexible, only residues 133–170 were used for the nativeness calculation. The dihedral angle criterion was also used in our secondary structure assignments. If the main-chain dihedral angles of a particular residue in the native helical region remain within $\pm 30^\circ$ of their native-state (ϕ, ψ) values during the simulation, this residue is considered to be still in the helical conformation. The helicity of a residue is defined as the percentage of occurrence of the helical conformation of this residue in the conformational ensemble. The core region used to calculate the radius of gyration (R_g^{core}) includes Ile135, Leu138, Leu139, Leu144, Ala146, Ile149, Leu158, Val163, and Leu167. The bin size for Q , length of helix (nHelix), rmsd, and R_g^{core} are 0.06, 1 residue, 0.45 Å, and 0.49 Å, respectively.

For the tertiary structure analysis, we mainly focused on the interhelical angle and the side-chain contacts between His166 and the rest of protein. The interhelical angle was calculated only if there were at least four consecutive residues assigned as helices in each helical region. The side chains of residue i and j ($j > i+3$) are considered to be in contact if the distance between their geometric center is less than 6.5 Å. The conformations within the lowest free energy contour lines of the global minimum and local minimum on the free energy surface are used for the analysis of interhelical angle.

RESULTS AND DISCUSSION

Unprotonated Fraction. To monitor the population of protonation states of the two histidine residues during the simulation, we plot the unprotonated fraction (S) as a function of time for the pseudotrajectories under 293 and 304 K (Figure 2). We chose these two trajectories because their temperatures are the closest to 298 K in the temperature space. A window of 1 ns was used to calculate S . Given the pK_a of His142 and His166,³ we calculated the theoretical values of S at different pH by solving the Henderson–Hasselbalch equation. Theoretically, $S = 0, 0.33, 0.68$, and 0.97 for His142 (at pH 5), His166 (at pH 5), His142 (at pH 7), and His166 (at pH 7), respectively. As seen in Figure 2, S converges to the theoretical values. If both His142 and His166 were fixed to the unprotonated state at pH 7 and to the protonated state at pH 5, the values of S would be 1 for both residues at pH 7 and 0 at pH 5. Our result demonstrates that the CPHMD

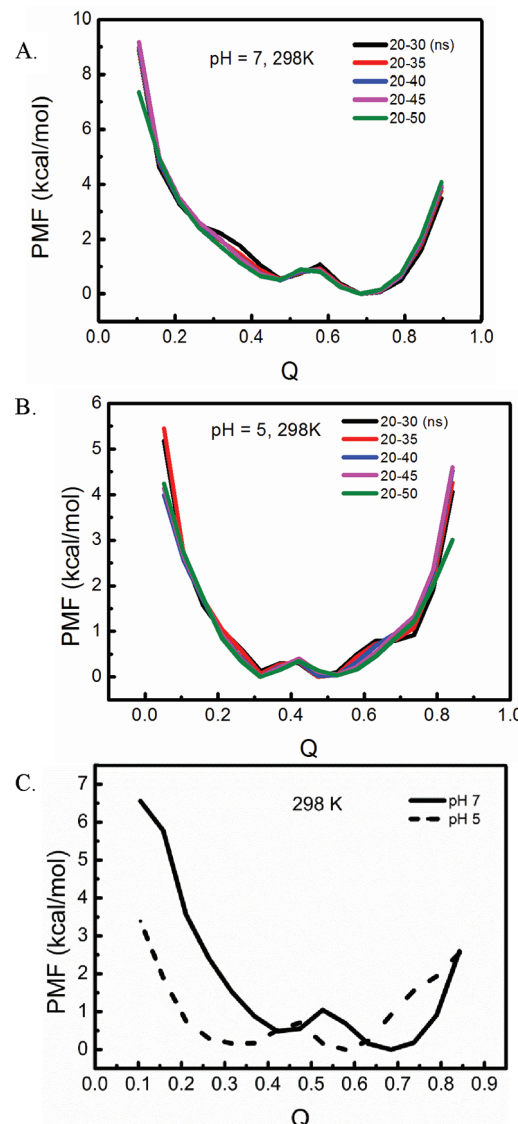


Figure 3. PMF as a function of nativeness (Q).

method correctly sampled the protonation states of the two histidine residues. This is also an indication of good convergence of our simulations.

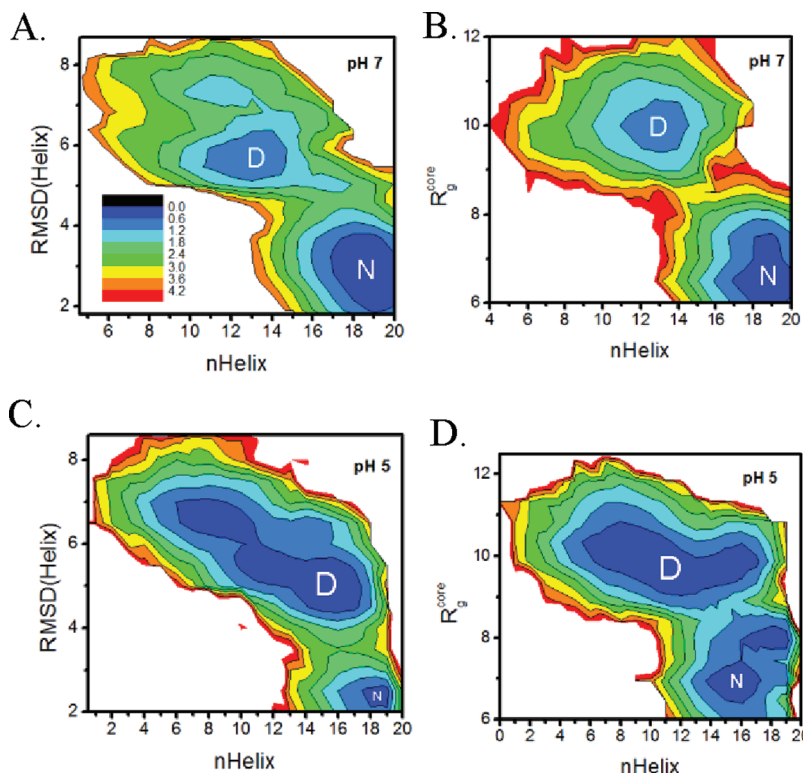


Figure 4. Free energy landscape at pH 7 (A and B) and pH 5 (C and D). nHelix denotes the length of helix. The unit of free energy is kcal/mol.

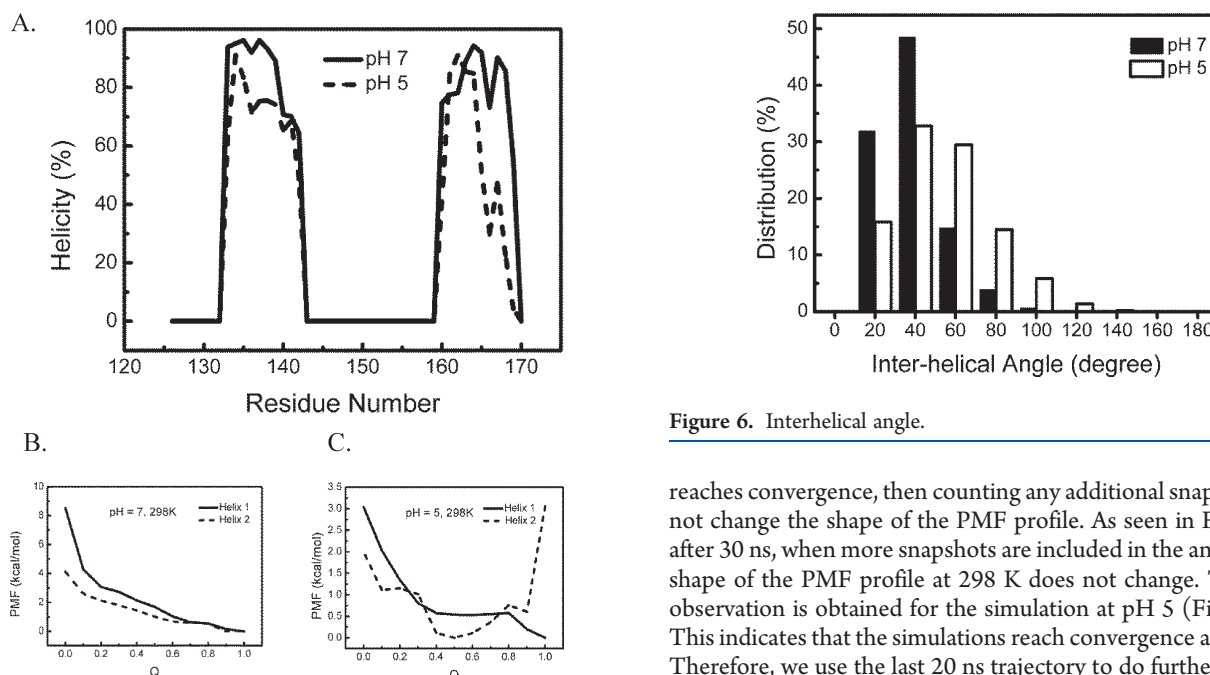


Figure 5. Secondary structure. (A) Weighted average helicity for each residue along the last 20 ns trajectories of all replicas. PMF as a function of Helix 1 helicity and as a function of Helix 2 helicity at pH 7 (B) and pH 5 (C).

Convergence Test. To further test the convergence of the replica exchange simulations, we plot the profile of PMF along the nativeness (Q) at different time frames. If the simulation

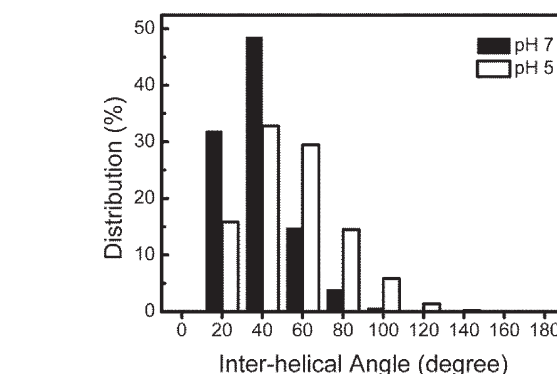


Figure 6. Interhelical angle.

reaches convergence, then counting any additional snapshots will not change the shape of the PMF profile. As seen in Figure 3A, after 30 ns, when more snapshots are included in the analysis, the shape of the PMF profile at 298 K does not change. The same observation is obtained for the simulation at pH 5 (Figure 3B). This indicates that the simulations reach convergence after 30 ns. Therefore, we use the last 20 ns trajectory to do further analysis. Following the convention, the unfolded state refers to the state where all of the amide protons are exposed for solvent exchange, while the denatured state is a nonnative free energy local minimum. Because the sampling in the low nativeness ($Q < 0.2$) is not enough, the unfolded state is not seen in the PMF profile. At pH 7, the global minimum is at $Q = 0.68 - 0.74$. A low barrier (~ 1 kcal/mol) separates the global minimum from a local minimum at $Q = 0.46 - 0.52$, which is a denatured state (Figure 3C). At pH 5, the profile of PMF shows one broad basin from $Q = 0.28 - 0.58$

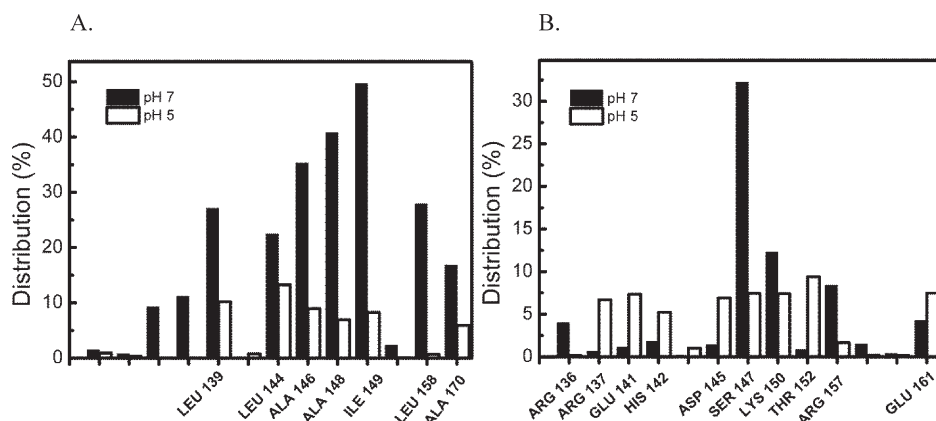


Figure 7. Side-chain–side-chain interactions between His 166 and the hydrophobic (A) and hydrophilic (B) residues.

using 1W4H as a reference (Figure 3C) with no substantial barrier. We also tried to use the solution structure resolved at pH 5 (2CYU⁵) as a reference; the resulting profile is similar to Figure 3C.

Free Energy Landscape. To obtain better descriptions of free energy surface, we tried combinations of various reaction coordinates. We find that the rmsd of the helices, the length of helix, and R_g^{core} are good order parameters to reflect the separations of different states. We do not intend to draw any conclusion on the folding mechanism solely based on the projected free energy surface because the complexity of the free energy landscape may be masked by the projection.²⁵ However, by comparing the shape of free energy surface along the same reaction coordinates for the simulations under different solvent conditions, we can uncover the solvent effects (at least along these reaction coordinates).

As seen in Figure 4A, the native-state basin is centered at about 3 Å of rmsd of helices with respect to the initial structure of the simulation at pH 7. Relatively large all-atom rmsd from the experimental NMR structure is seen in the traditional MD replica exchange simulations; approximately 60% of the conformations in the pseudo trajectory at 299 K exhibit above 5 Å all-atom rmsd in the work of Zhang et al.,^{21b} and only about 50% of native contacts are preserved at 300 K in the simulations of Pitera et al.^{21a} Even the traditional MD simulation of the native state by Settanni et al.⁴ shows larger than usual C^α rmsd. The maximum of the C^α rmsd goes to 4 Å in their work.⁴ The length of the helix in the native-state basin is from 17 residues to 20 residues (Figure 4A). Overall, the helical conformations in this basin are close to those in the NMR structure (1W4H). The denatured state at the neutral pH exhibits substantial loss in helical conformations. Its length of helix is only 11–14 residues. The radius of gyration of the core region increases to 10 Å, indicating that the core is loosely packed in the denatured state (Figure 4B). The barrier that separates the native state from the denatured state is 2–3 kcal/mol. Because the height of free energy barrier depends on the projection, attention should be paid to the comparison of the landscapes under different solvent conditions. At pH 5 (Figure 4C,D), the native-state basin is separated from the denatured state along the rmsd of helices/ R_g^{core} versus the length of helix (Figure 4C). However, the denatured state populates in a broad region: from 4.2 Å to 7 Å in rmsd of the helical region and from 6 residues to 17 residues in the length of helix. The height of the barrier between the native state and the denatured state on the projected surface along the rmsd of helical regions and the length of

helix is comparable to that at pH 7, but along other order parameters, such as Q and R_g^{core} versus nHelix, the barrier is significantly lower at pH 5 than that at pH 7 (Figures 3C and 4D).

Secondary Structure. To reveal the details of the secondary structure, we calculated the helicity which is the weighted average over the entire conformational ensemble collected in the last 20 ns of all replicas, for a total of 240 000 conformations (Figure 5A). At neutral pH, both Helix 1 and Helix 2 maintain their secondary structure integrity to a very high level, while at acidic pH, a severe secondary structure loss is seen at the C-terminus of Helix 2. This observation is in good agreement with that obtained from the C^α secondary shifts at pH 7.2 and pH 4.8 as well as that from the traditional MD simulations of the native state.^{3,4} Figure 5B shows the PMF as a function of Helix 1 helicity and as a function of Helix 2 helicity at neutral pH. The free energy minimum is located at 100% helicity for both helices at neutral pH. Under acidic pH (Figure 5C), the free energy minimum remains at 100% helicity of Helix 1, while the lowest free energy shifts to 50% helicity of Helix 2. Both the helicity analysis and the PMF profile demonstrate that the solvent conditions influence the secondary structure substantially.

Tertiary Structure. The two main helices adopt a parallel orientation in the native state (Figure 1). For the denatured state and the native state, we calculated the interhelical angle only if at least one turn of helix is present in each of the Helix 1 and Helix 2 regions. There are 35 150 conformations and 16 930 conformations satisfy this criterion at pH 7 and pH 5, respectively. The results shown in Figure 6 are weighted using PTWHAM²³ and renormalized. The distribution of interhelical angle at pH 5 is broader than that at neutral pH. The tail region of the distribution at pH 5 reaches 80–120°, which indicates the perpendicular orientation of the two helices.

We present the side-chain–side-chain interactions between His166 and the rest of the protein in Figure 7. This distribution is also the result of weighted average over the conformations generated in the last 20 ns of the simulations. At pH 7, His166 is in contact with a large number of hydrophobic residues (Leu139, Leu144, Ala146, Ala148, Ile149, Leu158, and Ala170), most of which are located in the loop region. It also interacts with two hydrophilic/charged residues on the loop, Ser147 and Lys150. At the acidic pH, it is unfavorable for the protonated His166 to remain in the hydrophobic environment. The side chains have to undergo rearrangements, which lead to the solvent-exposed conformation of His166. As shown in Figure 7B, the occurrence

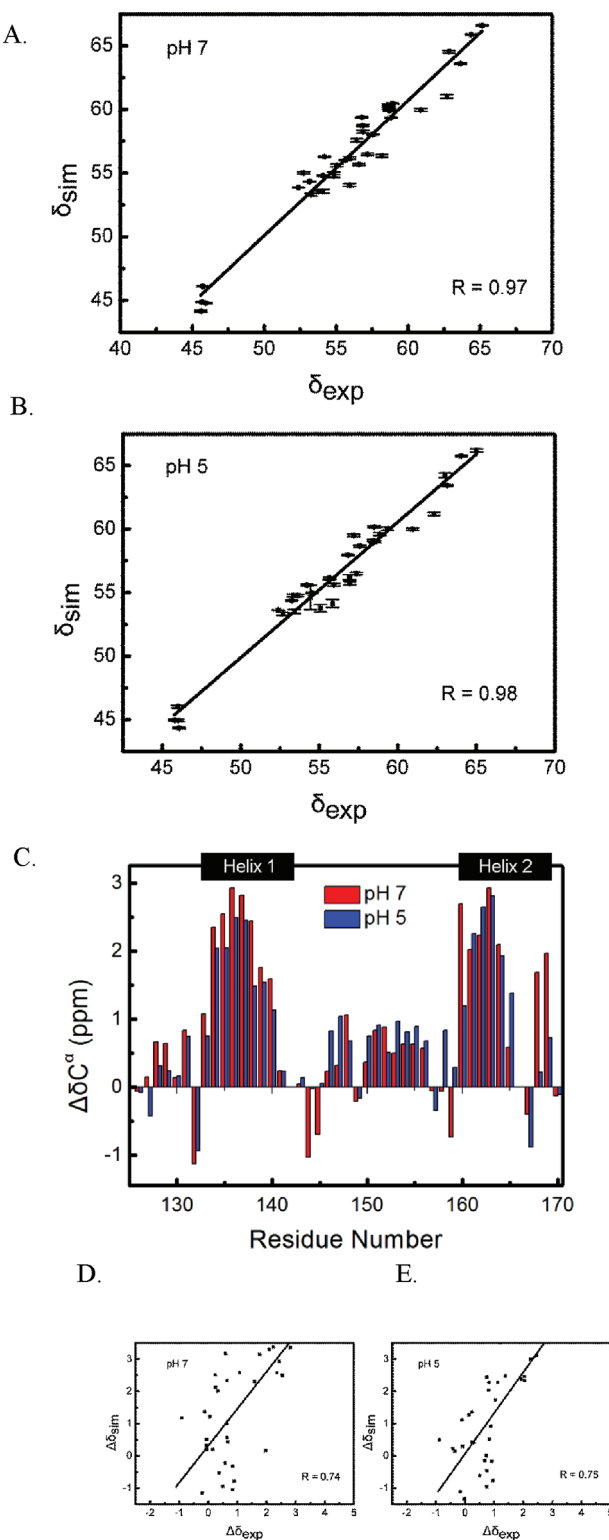


Figure 8. Chemical shift calculation. Weighted average chemical shifts over all of the conformations generated in the last 20 ns of the simulations at pH 7 (A) and pH 5 (B). C $^\alpha$ secondary chemical shifts (C). Correlation between the calculated C $^\alpha$ secondary chemical shifts and the experimental data for pH 7 (D) and pH 5 (E). The experimental data is presented in ref 3. Although our ionic strength at pH 5 is different from that used in the NMR experiment,³ we do not believe that the ionic strength at pH 5 in the implicit solvent model will affect our sampling significantly.

of each pair of side-chain contacts with His166 rarely exceeds 10%. The loss in the side-chain contacts between His166 and the loop increases the loop flexibility at acidic pH, which could be one of the causes of the broad distribution of interhelical angle at pH 5. It is not uncommon that the protonation state of histidine is responsible for protein loop conformational changes under acidic conditions. For example, it was found that the side-chain rearrangement of a key histidine residue under acidic pH leads to the relocation of internal fusion loop 2 of glycoprotein B from herpes simplex virus type 1.²⁶ Therefore, the solvent conditions not only influence the secondary structure, but also the tertiary structure.

Chemical Shift Calculation. We calculated the weighted average chemical shifts over all of the conformations generated in the last 20 ns of the simulations. As shown in Figure 8A,B, the calculated chemical shifts reproduce the experimental data very well with correlation coefficients of 0.98 and 0.97 at the neutral pH and the acidic pH, respectively. This level of correlation is comparable to that of the training set and the validation set used in SHIFTX.²⁴ The consistency between the calculated chemical shifts and the experimental data validates our constant pH simulations. The uncertainty in the calculated chemical shifts is less than the corresponding chemical shift value by 1–2 orders of magnitude. This also indicates good convergence of the simulation. The calculated C $^\alpha$ secondary shifts ($\Delta\delta C^\alpha$) are shown in Figure 8C, and the correlation between the calculated $\Delta\delta C^\alpha$ and the experimental data are presented in Figure 8D,E. The experimental C $^\alpha$ secondary shifts of BBL revealed a decrease in helicity at the C-terminus of Helix 2 under acidic pH.³ Our calculation reproduces the experimental results in a qualitative fashion. Although the calculated $\Delta\delta C^\alpha$ values are systematically less than the experimental data with the correlation coefficients of 0.74 and 0.75 at pH 7 and pH 5, respectively, we reproduce the trend of secondary structure integrity under different solvent conditions (comparing Figure 8C in this work and Figure 4 of ref 3).

The traditional MD simulations by Settanni et al. showed that the secondary structure of the native state varies with pH.⁴ Inspired by their work, we propose an interpretation of the observed low helicity at acidic pH from the free energy landscape point of view. At neutral pH, the native state is the predominant species at equilibrium. Hence, the C $^\alpha$ secondary shifts primarily reflect the native-state secondary structure, while at acidic pH, the denatured state has increased populations with lower helicity in Helix 2 with respect to its counterpart at the neutral pH. As a result, the observed chemical shifts at pH 5 may be due to the contributions from both the native state and the denatured state. Our chemical shift calculation validates this interpretation. However, we cannot exclude the native-state heterogeneity proposed by Fersht and co-workers^{3,4} because the shape of free energy surface depends on the ways of projection. The two scenarios—the equilibrium between the denatured state and the native state and the native-state heterogeneity—are likely to coexist.

The quality of the calculated NMR secondary chemical shifts depends on the accuracy of the algorithm or method used for the chemical shift prediction and the force field.²⁷ It has been found that different chemical shift prediction methods give appreciably different results of C $^\alpha$ secondary chemical shifts for the same set of simulated structures.²⁸ Like all simulation works, our simulations are inevitably limited by the force fields. For example, the helicity measured with backbone dihedral angles may be sensitive to the force fields. However, the relative stability between Helix 1 and Helix 2 seen in our work is in a good agreement with the

results of C^α secondary shifts.³ The salt effect is not explicitly treated in the implicit solvent model. In addition, the free energy surface depends on the choice of order parameters. A wiser choice of order parameters may result in a better defined denatured state. We tried various combinations of order parameters, yet, no better reaction coordinates have been found. However, attention should be focused on the change of free energy surface with the solvent conditions. Considering the simulation results under neutral pH with 0.2 M of salt as a control, the condition of acidic pH with no salt reshapes the free energy surface, leading to a broad denatured-state basin and a low barrier. With the control simulation, the bias caused by the force field is minimal.

CONCLUSIONS

Using CPHMD simulations combined with replica exchange, we have sampled the conformation space and protonation states of BBL. Overall, the barrier separating the native state and the denatured state is lower under the acidic pH than that under the neutral pH. The denatured-state basin is broad at pH 5. The acidic pH condition shifts the equilibrium between the denatured state and the native state in favor of the denatured state. Under the acidic pH condition, the experimental measurements have significant contributions from the denatured state. Therefore, the interpretation of any experimental data under this condition should take into account the denatured state. Our simulations are supported by the fact that our data reproduce the loss in the helical content of Helix 2 detected by the NMR experiment.³

ASSOCIATED CONTENT

Supporting Information. Random walk in the rmsd space and temperature space as well as the unfolding and refolding events during the simulations. This material is available free of charge via the Internet at <http://pubs.acs.org>.

AUTHOR INFORMATION

Corresponding Author

*E-mail: shuo@clarku.edu.

ACKNOWLEDGMENT

This work is funded by National Institutes of Health (1R01-GM088326). We thank Dr. Fersht for providing their chemical shift data. We are very grateful to Drs. M. Feig, J. Khandogin, and W. Im for their help with the MMTSB Tool Set and phmd and gbsw modules in CHARMM. We also thank Dr. R. Zhou for helpful discussions.

REFERENCES

- Mande, S. S.; Sarfaty, S.; Allen, M. D.; Perham, R. N.; Hol, W. G. *Structure* **1996**, *4* (3), 277–86.
- Ferguson, N.; Sharpe, T. D.; Schartau, P. J.; Sato, S.; Allen, M. D.; Johnson, C. M.; Rutherford, T. J.; Fersht, A. R. *J. Mol. Biol.* **2005**, *353* (2), 427–46.
- Arbely, E.; Rutherford, T. J.; Sharpe, T. D.; Ferguson, N.; Fersht, A. R. *J. Mol. Biol.* **2009**, *387* (4), 986–92.
- Settanni, G.; Fersht, A. R. *J. Mol. Biol.* **2009**, *387* (4), 993–1001.
- Sadqi, M.; Fushman, D.; Munoz, V. *Nature* **2006**, *442* (7100), 317–21.
- Pettersen, E. F.; Goddard, T. D.; Huang, C. C.; Couch, G. S.; Greenblatt, D. M.; Meng, E. C.; Ferrin, T. E. *J. Comput. Chem.* **2004**, *25* (13), 1605–12.
- Garcia-Mira, M. M.; Sadqi, M.; Fischer, N.; Sanchez-Ruiz, J. M.; Munoz, V. *Science* **2002**, *298* (5601), 2191–5.
- Desai, T. M.; Cerminara, M.; Sadqi, M.; Munoz, V. *J. Biol. Chem.* **2010**, *285* (45), 34549–56.
- Fan, J.; Duan, M.; Li, D. W.; Wu, H.; Yang, H.; Han, L.; Huo, S. *Biophys. J.* **2011**, *100* (10), 2457–65.
- Cho, S. S.; Weinkam, P.; Wolynes, P. G. *Proc. Natl. Acad. Sci. U.S.A.* **2008**, *105* (1), 118–23.
- (a) Sham, Y. Y.; Muegge, I.; Warshel, A. *Biophys. J.* **1998**, *74* (4), 1744–53. (b) Simonson, T.; Archontis, G.; Karplus, M. *J. Phys. Chem. B* **1999**, *103*, 6142–6156. (c) Warshel, A.; Aqvist, J. *Annu. Rev. Biophys. Biomol. Eng.* **1991**, *20*, 267–98.
- (a) Mongan, J.; Case, D. A. Biomolecular simulations at constant pH. *Curr. Opin. Struct. Biol.* **2005**, *15* (2), 157–63. (b) Meng, Y.; Roitberg, A. E. *J. Chem. Theory Comput.* **2010**, *6* (4), 1401–1412. (c) Stern, H. A. *J. Chem. Phys.* **2007**, *126* (16), 164112.
- (a) Lee, M. S.; Freddie, R.; Salsbury, J.; Charles, L.; Brooks, I. *Proteins: Struct., Funct., Bioinf.* **2004**, *56*, 738–752. (b) Khandogin, J.; Brooks, C. L. *Biophys. J.* **2005**, *89* (1), 141–157.
- Brooks, B. R.; Brooks, C. L., III; Mackerell, A. D., Jr.; Nilsson, L.; Petrella, R. J.; Roux, B.; Won, Y.; Archontis, G.; Bartels, C.; Boresch, S. *J. Comput. Chem.* **2009**, *30* (10), 1545–614.
- Kong, X.; Brooks, C. L. *J. Chem. Phys.* **1996**, *105*, 2414–2423.
- Mackerell, A. D., Jr. *J. Comput. Chem.* **2004**, *25* (13), 1584–604.
- (a) Chen, J.; Im, W.; Brooks, C. L., III. *J. Am. Chem. Soc.* **2006**, *128* (11), 3728–36. (b) Im, W.; Lee, M. S.; Brooks, C. L., III. *J. Comput. Chem.* **2003**, *24* (14), 1691–702.
- Sugita, Y.; Okamoto, Y. *Chem. Phys. Lett.* **1999**, *314*, 141–151.
- Ma, L.; Ahmed, Z.; Asher, S. A. *J. Phys. Chem. B* **2011**, *115* (14), 4251–8.
- Feig, M.; Karanicolas, J.; Brooks III, C. L. *J. Mol. Graphics Modell.* **2004**, *22* (5), 377–395.
- (a) Pitera, J. W.; Swope, W. C.; Abraham, F. F. *Biophys. J.* **2008**, *94* (12), 4837–46. (b) Zhang, J.; Li, W.; Wang, J.; Qin, M.; Wang, W. *Proteins* **2008**, *72* (3), 1038–47.
- Ryckaert, J. P.; Ciccotti, G.; Berendsen, H. J. C. *J. Comput. Phys.* **1977**, *23*, 327–341.
- Chodera, J. D.; Swope, W. C.; Pitera, J. W.; Seok, C.; Dill, K. A. *J. Chem. Theory Comput.* **2007**, *3* (1), 26–41.
- Neal, S.; Nip, A. M.; Zhang, H.; Wishart, D. S. *J. Biomol. NMR* **2003**, *26* (3), 215–40.
- Krivorov, S. V.; Karplus, M. *Proc. Natl. Acad. Sci. U.S.A.* **2004**, *101* (41), 14766–70.
- Stampfer, S. D.; Lou, H.; Cohen, G. H.; Eisenberg, R. J.; Heldwein, E. E. *J. Virol.* **2010**, *84* (24), 12924–33.
- Li, D.-W.; Bruschweiler, R. *J. Phys. Chem. Lett.* **2010**, *1*, 246–248.
- Reddy, A. S.; Wang, L.; Lin, Y. S.; Ling, Y.; Chopra, M.; Zanni, M. T.; Skinner, J. L.; De Pablo, J. J. *Biophys. J.* **2010**, *98* (3), 443–51.